

A High-Rate V_2O_5 Hollow Microclew Cathode for an All-Vanadium-Based Lithium-Ion Full Cell

Pengfei Zhang, Luzi Zhao, Qinyou An, Qiulong Wei, Liang Zhou, Xiujuan Wei, Jinzhi Sheng, and Liqiang Mai*

V_2O_5 hollow microclews (V_2O_5 -HMs) have been fabricated through a facile solvothermal method with subsequent calcination. The synthesized V_2O_5 -HMs exhibit a 3D hierarchical structure constructed by intertangled nanowires, which could realize superior ion transport, good structural stability, and significantly improved tap density. When used as the cathodes for lithium-ion batteries (LIBs), the V_2O_5 -HMs deliver a high capacity (145.3 mAh g^{-1}) and a superior rate capability (94.8 mAh g^{-1} at 65 C). When coupled with a lithiated Li_3VO_4 anode, the all-vanadium-based lithium-ion full cell exhibits remarkable cycling stability with a capacity retention of 71.7% over 1500 cycles at 6.7 C. The excellent electrochemical performance demonstrates that the V_2O_5 -HM is a promising candidate for LIBs. The insight obtained from this work also provides a novel strategy for assembling 1D materials into hierarchical microarchitectures with anti-pulverization ability, excellent electrochemical kinetics, and enhanced tap density.

1. Introduction

Lithium-ion batteries (LIBs) have attracted considerable interests in energy storage systems due to their various advantages such as high working voltage, high energy density, and long lifespan.^[1–7] However, their large-scale commercialization in electric vehicles and hybrid electric vehicles is still hindered by their poor rate performance and safety issue, which are mainly related to the electrode materials.^[8–13] In this regard, substantial research efforts have been focused on elaborate exploration and rational design of high-performance electrode materials.^[14,15]

Among the cathode materials, V_2O_5 , with feasible lithium-ion intercalation features, has aroused widespread attention

because of its high output voltage, low cost, abundant resource, and high energy density.^[16–21] However, it still suffers from poor cycling performance and rate capability due to the sluggish electric conductivity and the low lithium-ion diffusion kinetics.^[22,23] In recent years, constructing various nanostructures, such as nanorods,^[24,25] nanobelts,^[26] nanowires,^[27,28] porous structures,^[29] and nanoparticles,^[30] has been demonstrated as an effective strategy to shorten the lithium-ion diffusion distance and improve the electrochemical kinetics.^[22,31] Song et al. synthesized the unique mesoporous V_2O_5 nanosheets by a facile hydrothermal method. These V_2O_5 nanosheets exhibit ultrastable capacity retention and excellent rate capability, maintaining a reversible capacity of 118 mAh g^{-1} at 6000 mA g^{-1} after 1000 cycles.^[32] Nonetheless, many associated problems occur including low tap density and increased side reactions when the size of the electrode material is reduced to nanometer scale.^[33] The low tap density results in low volumetric energy density and thick electrode at high mass loading, making it hard to maintain the electronic and ionic pathways during cycling.^[34] Besides, the extended electrode/electrolyte contact significantly increases the side reactions, resulting in safety issues and poor cycling performance.^[35] The fabrication of high level organized hierarchical superstructures composed of nanosized building

P. F. Zhang, L. Z. Zhao, Prof. Q. Y. An, Q. L. Wei, Prof. L. Zhou, X. J. Wei, J. Z. Sheng, Prof. L. Q. Mai
State Key Laboratory of Advanced Technology for Materials Synthesis and Processing
Wuhan University of Technology
Hubei, Wuhan 430070, P. R. China
E-mail: mlq518@whut.edu.cn
DOI: 10.1002/smll.201503214



blocks provides a feasible strategy to overcome these problems because the superstructures could offer exceptional advantages of both the nanosized primary particles and micrometer-sized assemblies.^[18,33,34] Among the superstructures, the hierarchical hollow microsphere has attracted great interests because of its unique characteristics.^[36–39] The nanoscale building blocks of the microspheres facilitate the transport of lithium ions and electrons. And the porous shells and the void space within the hollow microspheres ensure the efficient electrolyte penetration and increase the contact area between the electrode and electrolyte.^[36] Furthermore, the microsized particles might suppress aggregation of primary nanoparticles, providing good structural integrity of the electrode.^[37,38] In addition, the void can alleviate localized volume change during the Li^+ intercalation/deintercalation process.^[39]

Herein we present an all-vanadium-based lithium-ion full cell consisting of a lithiated Li_3VO_4 anode and a V_2O_5 hollow microclew (V_2O_5 -HM) cathode for the first time, obtaining the comparable performance compared to the commercialized materials and excellent cycling stability at high rate. The unique V_2O_5 -HMs are successfully synthesized by a facile solvothermal method followed by calcination. Constructed by intertangled nanowires, the V_2O_5 -HMs not only inherit the nanowire features with short ionic and electronic transport pathways but also significantly improve the tap density due to the 3D hierarchical microstructure. This strategy has the potential to be extended to the assembly of various 1D materials into optimized microstructures with advanced physical/chemical properties. And the fabrication of both anode and cathode materials from the same source is a way to simplify the process of material synthesis and take advantage of abundant resources adequately, as well as allow for

convenient capacity matching and optimal capacity of the full cell.^[40,41] And these could be regarded as a significant exploration to develop the low-cost and high-performance full cell via a facile and energy-saving approach.

2. Results and Discussion

2.1. Morphology and Structure

The crystal phase of the samples is investigated by X-ray diffraction (XRD) (Figure 1a). The V_2O_5 -HM precursor exhibits the amorphous structure and converts into crystalline V_2O_5 (JCPDF card No. 01-089-0611) after calcination. As depicted in Figure 1b,c, the V_2O_5 -HM precursor is composed of microclews constructed by intertangled nanowires. The average diameter of the secondary structure is about 7 μm . After calcination in air, the microclew structure is well maintained (Figure 1d). From the transmission electron microscopy (TEM) image, a hollow cavity can be clearly observed at the center of the V_2O_5 microclew (Figure 1e, S1a,b, Supporting Information). Some fine structures with the nanowire morphology are also observed on the surface of the microclew (inset of Figure 1e), indicating that the V_2O_5 -HMs consist of the intertangled nanowires. The high-resolution TEM (HRTEM) image (Figure 1f) shows lattice fringes with a spacing of 3.4 \AA , which is associated with the (110) plane of V_2O_5 . As determined by N_2 -sorption (Figure S2, Supporting Information), the V_2O_5 -HMs hold a Brunauer–Emmett–Teller (BET) surface area of 20 $\text{m}^2 \text{g}^{-1}$ and a pore volume of 0.15 $\text{cm}^3 \text{g}^{-1}$. The pores are mainly contributed from the interstices among the assembled nanowires. The Raman spectrum of V_2O_5 -HMs is shown in Figure S3 (Supporting

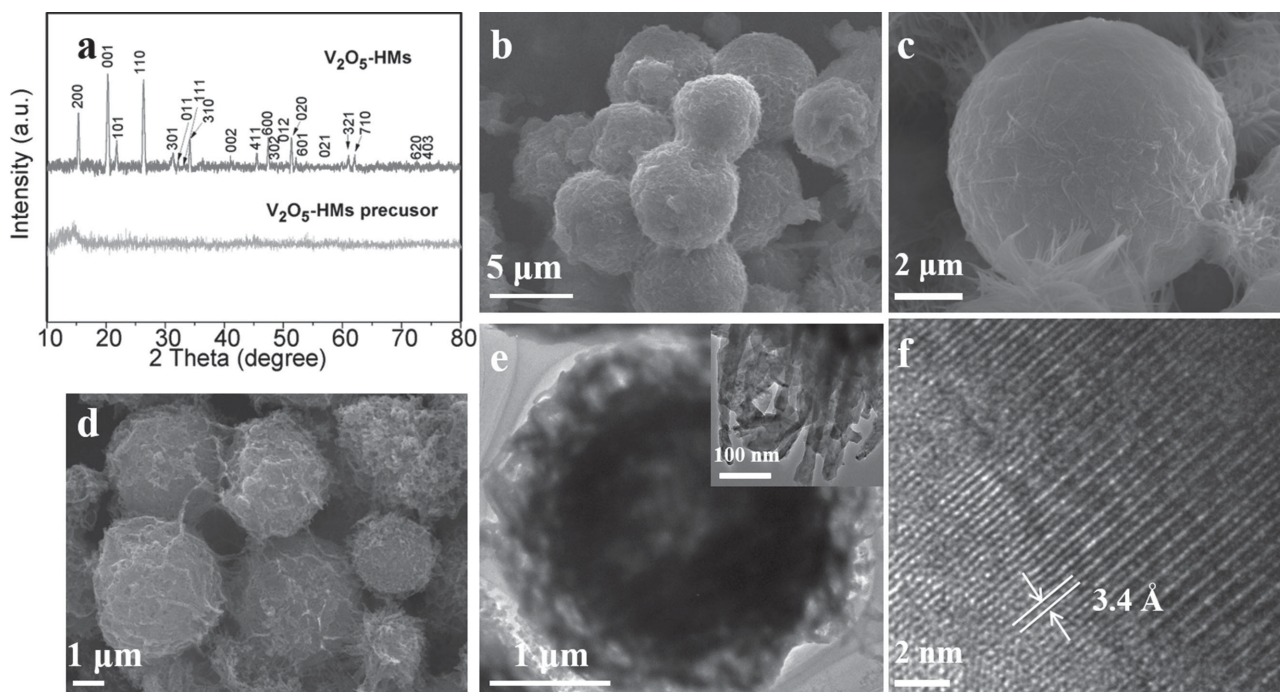
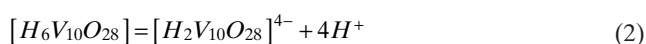
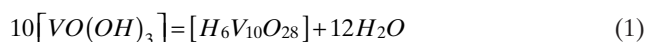


Figure 1. a) XRD of V_2O_5 -HMs and the precursor, b,c) SEM images of V_2O_5 -HM precursor, d) SEM image of V_2O_5 -HMs, and e,f) TEM and HRTEM images of V_2O_5 -HMs. The inset of (e) is the magnified image of the fine structure.

Information). The bands below 1000 cm^{-1} come from V_2O_5 .^[42] The characteristic bands for carbonaceous materials, which usually appear at ≈ 1350 and $\approx 1590\text{ cm}^{-1}$, cannot be observed, unambiguously demonstrating that no carbon residue exists after calcination. It should be pointed out that the V_2O_5 -HMs exhibit a significantly improved tap density than the V_2O_5 nanowires (V_2O_5 -NWs). After packing the same mass of V_2O_5 -HMs and nanowires in glass tubes, the volume of V_2O_5 -HMs is just 44% to that of nanowires (Figure S4, Supporting Information).

2.2. Formation Mechanism Analysis

To explore the formation process of the V_2O_5 -HMs, time-dependent experiments are carried out (Figure 2, S5-8, Supporting Information). First, V_2O_5 -NW network is obtained after an ultrasonic process (Figure 2a). During the solvothermal reaction, the nanowires aggregate and intertangle gradually, and then self-roll into microclews (Figure 2b-d). Finally, after calcinating in air, the V_2O_5 -HMs are attained (Figure 1d). Based on the above results, a proposed growth mechanism is illustrated in Figure 3. It has been reported that there is an ionization balance in the V_2O_5 sol ($\text{pH} > 2$)^[43-46] which can be illustrated as follows



The tris (hydroxymethyl) methylaminomethane (THAM) would also ionize in solution as follows^[47,48]



Due to the electrostatic interactions between the $[\text{H}_2\text{V}_{10}\text{O}_{28}]^{4-}$ species and the $[\text{NH}_3\text{C}(\text{CH}_3\text{OH})_3]^+$ species, the $[\text{NH}_3\text{C}(\text{CH}_3\text{OH})_3]^+$ absorbs on the vanadium species, which causes the coagulation of the system and formation of the nanowires.^[49] To minimize the surface energy, the nanowires undergo a crimping and self-roll process, forming nanofibrous microclews with hollow cavities at the center.^[50,51] With the nanowires getting closer, the repulsion between the $[\text{NH}_3\text{C}(\text{CH}_3\text{OH})_3]^+$ species absorbed on adjacent nanowires dominates, avoiding the further aggregation of the nanowires.^[52] After removing the organic species from the microclews during calcination, the structural integrity of the microclews can be well maintained, while pores or interstices can be formed between the nanowires. In order to understand the function of the THAM in this process, controlled experiments with different amount of THAM are carried out. No product is attained without the addition of THAM before (Figure S9, Supporting Information) and after (Figure S10, Supporting Information) the solvothermal reaction, which further proves that the THAM acts as a coagulation agent in this reaction. When the amount of the THAM is decreased to 1.0 g, V_2O_5 microspheres are obtained. The V_2O_5 microspheres are amorphous and change into crystalline V_2O_5 (V_2O_5 -Ms) after calcination (Figure S11a, Supporting Information). The SEM images (Figure S11b,c, Supporting Information) indicate that the V_2O_5 microspheres possess a much smoother surface and partly break into small pieces after thermal treatment. The reason for the formation of V_2O_5 -Ms can be explained as follows: with less THAM added, the repulsion between neighboring nanowires becomes much weaker, and the nanowires aggregate more seriously than that

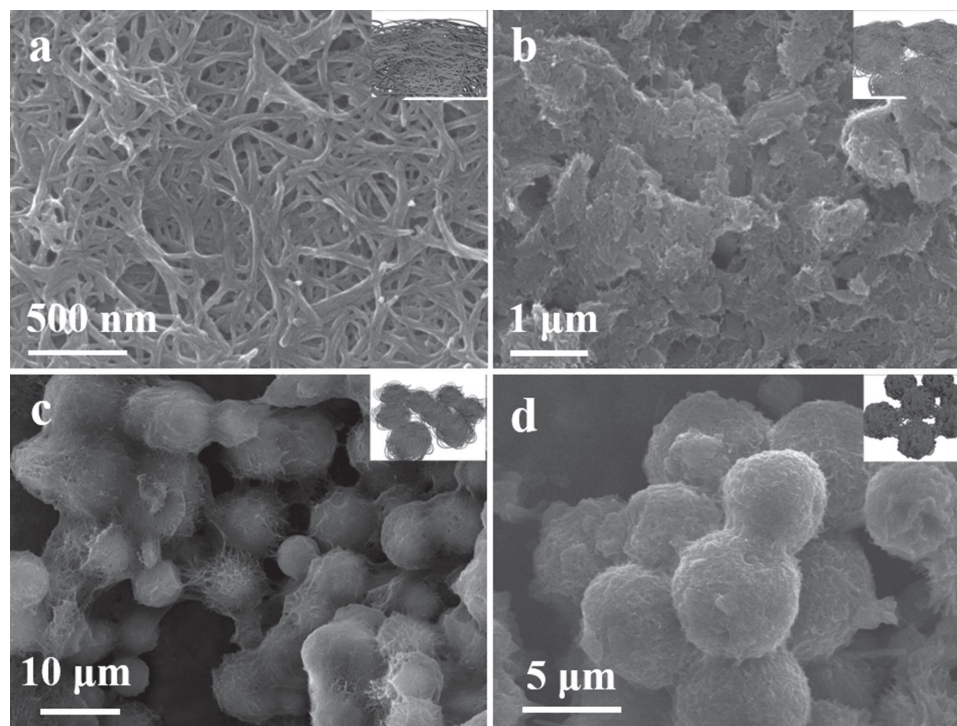


Figure 2. SEM images of V_2O_5 -HM precursor obtained at different times: a) 0 min, b) 40 min, c) 80 min, and d) 120 min.

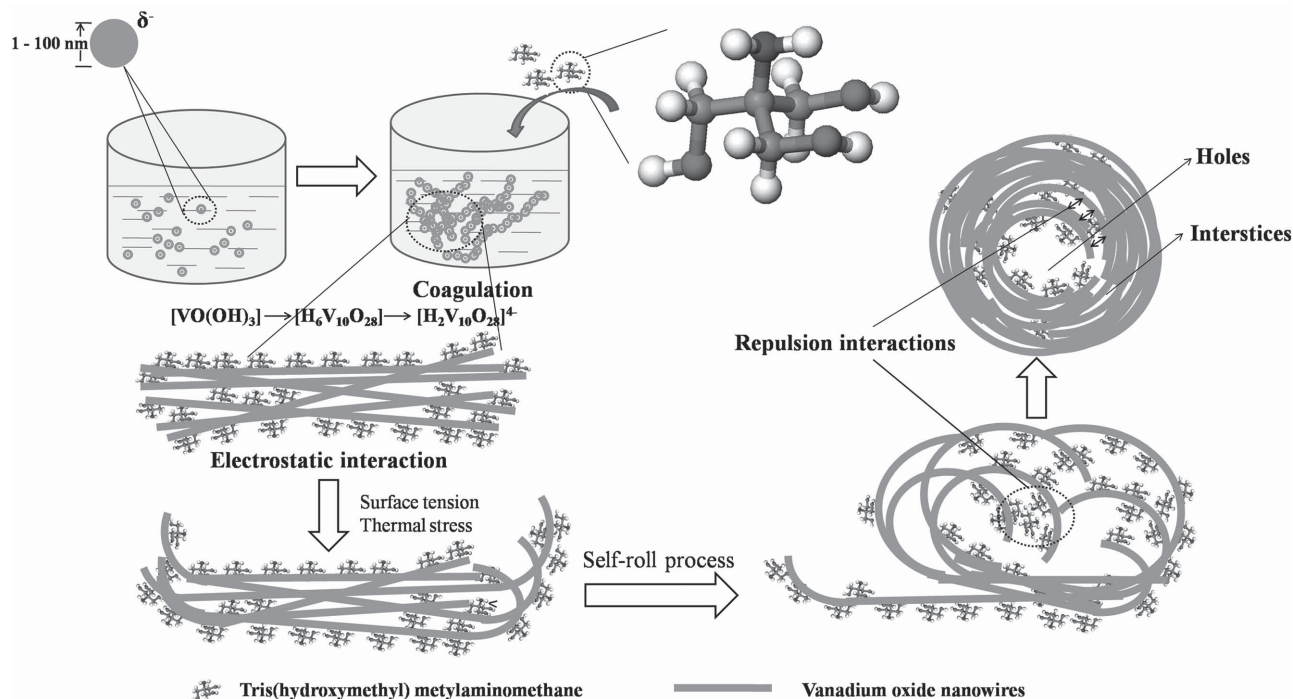


Figure 3. Proposed formation mechanism of the V_2O_5 -HM precursor.

of V_2O_5 -HMs, forming smooth microspheres without cavities (Figure S11d, Supporting Information). With the amount of THAM increasing, more and more nanorods are observed (Figure S12, Supporting Information). This is due to the formation of more $[NH_3C(CH_3OH)_3]^+$ cations, which absorb on the vanadium species and make the repulsion between neighboring nanowires stronger. As a result, more and more isolated vanadium oxide nanowires tend to grow into nanorods, rather than forming microclews during the solvothermal process.

2.3. Half-Cell Electrochemical Characterization

Half cells (2016-type coin cell) with metallic lithium as the anode are assembled to investigate the electrochemical properties of the V_2O_5 -HM electrode. Cyclic voltammogram of the V_2O_5 -HMs is measured at a scan rate of 0.2 mV s^{-1} in a potential range from 2.4 to 4.0 V (Figure 4a). The potential range of 2.4–4.0 V is chosen to measure the electrochemical performance so as to avoid the irreversible structural modifications, which makes the long-term cycling stability possible, meanwhile, a comparable capacity compared to the commercialized cathode materials can be obtained. Furthermore, the energy density of electrode is relatively high due to the high output voltage of V_2O_5 during the α - ϵ , ϵ - δ transition. A couple of cathodic/anodic peaks appear at potentials of 3.31/3.50 V, belonging to the phase transformations between α - V_2O_5 and ϵ - $Li_{0.5}V_2O_5$, while the peaks at 3.01 and 3.35 V correspond to the phase transformations between ϵ - $Li_{0.5}V_2O_5$ and δ - LiV_2O_5 .^[31,53] To investigate the structural advantages of V_2O_5 -HMs during the electrochemical process, the performance of

the V_2O_5 -NWs prepared by the solvothermal method and calcination in air (Figure S13b, Supporting Information) and the V_2O_5 -Ms are also measured. The cycling performances of V_2O_5 -HMs, V_2O_5 -Ms, and V_2O_5 -NWs at 0.67 C are shown in Figure 4b. The initial discharge capacities of V_2O_5 -HMs, V_2O_5 -Ms, and V_2O_5 -NWs are 145.3, 141.7, and 146.8 mAh g^{-1} (theoretical capacity of 147 mAh g^{-1} based on one lithium insertion per formula unit), respectively. The initial discharge capacity of V_2O_5 -NWs is higher than that of V_2O_5 -HMs owing to its more exposed surface area ($21.3 \text{ m}^2 \text{ g}^{-1}$ vs $20.2 \text{ m}^2 \text{ g}^{-1}$). And the capacity drops to 137.2, 119.7, and 123.5 mAh g^{-1} after 50 cycles, corresponding to a capacity retention of 94.4%, 84.5%, and 84.1%, respectively. When the rate increases to 13.3 C (Figure 4c), the initial discharge capacities of V_2O_5 -HMs, V_2O_5 -Ms, and V_2O_5 -NWs are 111.6, 71.7, and 120.0 mAh g^{-1} , respectively. Although the initial capacity of V_2O_5 -HMs is slightly lower than that of V_2O_5 -NWs, after several cycles, the V_2O_5 -HMs hold the highest capacity during the rest cycles. After 26 cycles, the discharge capacity of the V_2O_5 -HMs is 129.3 mAh g^{-1} , which is higher than those of the V_2O_5 -NWs (122.2 mAh g^{-1}) and the V_2O_5 -Ms (96.1 mAh g^{-1}). The rise of capacity at the beginning is attributed to the gradual penetration of electrolyte into the sample interior.^[54] The rate capability of the three samples is shown in Figure 4d, and the V_2O_5 -HMs exhibit excellent cycling response to various rates. Even discharged at a very high rate of 65 C, a high capacity of 94.8 mAh g^{-1} is attained for the V_2O_5 -HMs (Figure 4d, S14, Supporting Information), which is about five times larger than those of the V_2O_5 -Ms (16.2 mAh g^{-1}) and the V_2O_5 -NWs (18.1 mAh g^{-1}). Notably, when the rate is reduced back to 1 C, the capacity of the V_2O_5 -HMs can be fully recovered, attesting its good

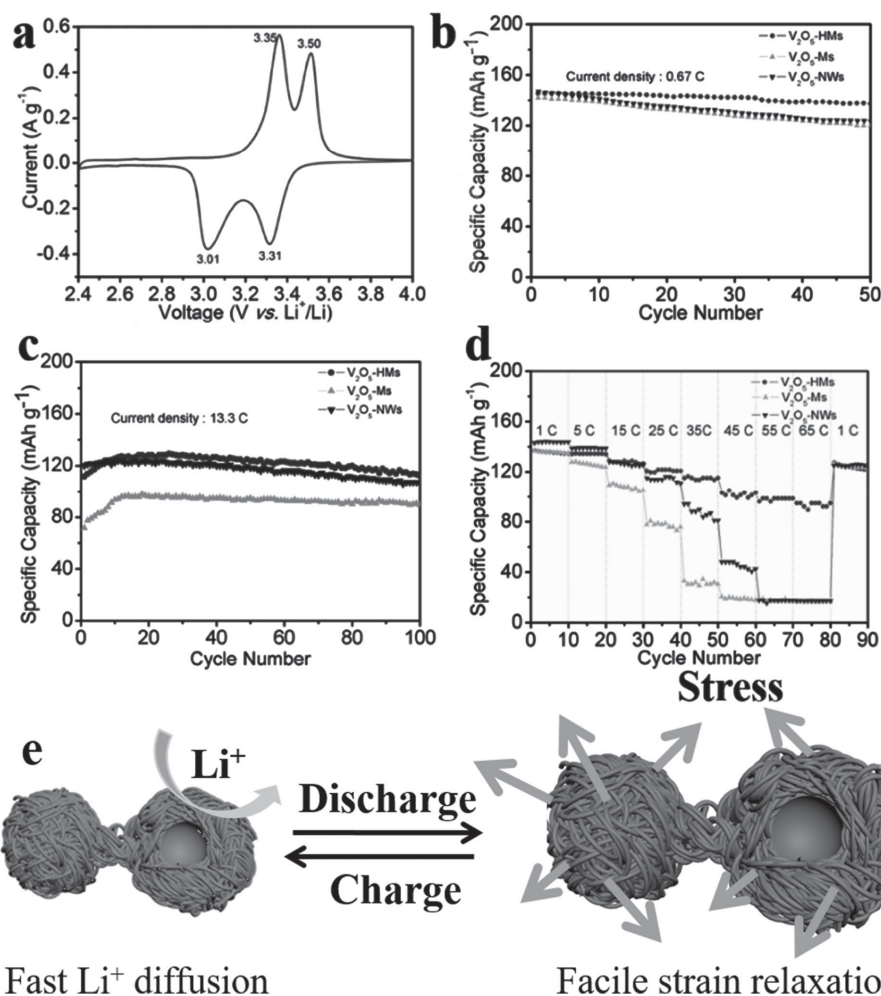


Figure 4. a) The cyclic voltammograms of V_2O_5 -HMs at a scan rate of 0.2 mV s^{-1} . b) Cyclic performance of V_2O_5 -HMs, V_2O_5 -Ms, and V_2O_5 -NWs at 0.67 C . c) Cyclic performance of V_2O_5 -HMs, V_2O_5 -Ms, and V_2O_5 -NWs at 13.3 C . d) Rate capability of V_2O_5 -HMs, V_2O_5 -Ms, and V_2O_5 -NWs at various rates. e) Schematic illustration of the V_2O_5 -HMs during charge/discharge. The HM structure shortens the ion-diffusion pathway and provides a facile strain relaxation during lithiation/delithiation.

reversibility. The superior rate capability of V_2O_5 -HMs can be attributed to their robust architecture with excellent mechanical integrity, which keeps efficient and large contact area between the active sites and electrolytes, as well as short Li^+ ion diffusion distances. SEM images of the three electrodes before and after the rate measurements are in accordance with the results above (Figures S13 and S15, Supporting Information). The unique microclew structure of the V_2O_5 -HMs is well maintained after cycling at high rate, while the structure of the V_2O_5 -Ms and the V_2O_5 -NWs is almost destroyed during cycling. The superior anti-pulverization and anti-aggregation abilities of the V_2O_5 -HMs can be ascribed to their 3D hierarchical hollow structure constructed by intertangled nanowires. The electrochemical impedance spectra are employed to provide further insights about the electrochemical process of the electrodes (Figure S16, Supporting Information). The Nyquist plots show that the contact and charge transfer resistance (R_{ct}) of the V_2O_5 -HMs is obviously lower than those of the other two samples, suggesting the more facile charge-transfer process on the electrode/electrolyte interface in V_2O_5 -HMs.

It is ascribed to the effective contact between the electrode and the electrolytes, as well as a short ion-electron transfer even under the greatly high rate, maintained by the robust architecture of V_2O_5 -HMs.

The impressive electrochemical performance of the V_2O_5 -HMs is ascribed to their unique HM structure constructed by intertangled nanowires. More specifically, first, the nanowire building blocks greatly promote the electron transport and lithium-ion diffusion kinetics by shortening their pathways. In addition, the nanowires also alleviate the strain effectively during the lithium-ion intercalation.^[55,56] Second, the pores or interstices between the nanowires increase the electrode–electrolyte interface, which ensures a much more effective utilization of the electrode materials and facilitates the intercalation of the lithium-ion from various direction of the microclews.^[57–61] Third, the hollow structure effectively buffers the unavoidable volume change during the lithium-ion insertion and extraction processes (Figure 4e), decreasing the pulverization of the V_2O_5 -HM active materials, further improving the cycling stability and rate performance.^[62]

0.2–3.0 V. And then it is discharged to 0.2 V vs Li⁺/Li with two lithium ions insertion.^[31] The all-vanadium-based lithium-ion full cell is then assembled with a slight excess (5%–10%) of anode to make full use of the cathode material. Figure 5c shows this full cell operates at the potential range from 1.0 to 3.5 V with a voltage profile matching, which is expected by the combination of the V₂O₅-HM cathode and the Li₃VO₄-CNT composite anode. Figure 5d shows that the full cell delivers a capacity of 138.6 mAh g⁻¹ (the capacity is calculated based on the mass of the V₂O₅-HM cathode) at the first discharge and retains about 100 mAh g⁻¹ after 200 cycles at 0.67 C, corresponding to capacity retention of 71.3%. Moreover, except for the initial few cycles, the coulombic efficiency of the full cell reaches more than 97%. As shown in Figure 5e, the V₂O₅-HM/Li₃VO₄-CNT full cell exhibits excellent rate performance. Even at a very high rate of 20 C, a high capacity of 70 mAh g⁻¹ can still be attained. And it also shows great cycling ability with only 28.3% capacity loss after 1500 cycles at rate 6.7 C (Figure 5f). The superior electrochemical properties of the all-vanadium-based lithium-ion full cell are also attributed to the elaborate selection and matching of electrode materials.

3. Conclusion

A facile solvothermal reaction followed by calcination is developed for the synthesis of V₂O₅-HMs. The synthesized V₂O₅-HMs show excellent cycling performance and rate capability with 94.8 mAh g⁻¹ at a high rate of 65 C in the half-cell testing. All-vanadium-based lithium-ion full cells are assembled using V₂O₅-HMs as the cathode and Li₃VO₄-CNTs as the anode for the first time. The V₂O₅-HM/Li₃VO₄-CNT full cell retains 71.7% of its initial capacity after 1500 cycles at 6.7 C. The good cycling stability and rate performance is attributed to the unique V₂O₅-HM structure with fast electrolyte penetration, short lithium ion/electron transport, and effective pulverization suppression. When compared with disordered nanowires, the V₂O₅-HMs exhibit significantly improved tap density. Our work demonstrates that the V₂O₅-HMs constructed by intertwined nanowires are promising for LIB application. Further optimization and development of the all-vanadium-based design and fabrication will bring about new opportunities in high-performance energy storage devices. It is envisaged that our strategy of designing novel superstructures by the assembly of 1D building blocks can be generally applied to other materials for boosting the electrochemical performances.

4. Experimental Section

Materials Synthesis: The V₂O₅-HMs are simply achieved by a solvothermal reaction followed by a calcination process in air. First, the V₂O₅ sols were prepared by a melt quenching process according to previous work.^[68] In brief, the V₂O₅ powder (30 g) was placed in a ceramic crucible and heated in air at 800 °C for 20 min at a rate of 10 °C min⁻¹, resulting in a molten liquid. Then, the molten liquid was quickly poured into distilled water (1 L)

with stirring, and suspension was obtained. The suspension was heated to the boiling point of water beforehand and then cooled to room temperature naturally. Finally, the suspension was filtered and the brownish V₂O₅ sols were obtained. The concentration of the V₂O₅ sols was calculated by weighting the residual mass after drying the sols in 180 °C for 1 d. To adjust the concentration of sols, moderate distilled water was slowly added and the sols were stirred for another 1 h. In a typical synthesis, 10 mL 0.05 mol L⁻¹ of V₂O₅ sol is added into 50 mL of 2-propyl alcohol (IPA) in a Teflon-lined stainless steel autoclave (100 mL) with 2.0 g of THAM added sequentially. The mixture was then ultrasonicated at 50 Hz for 30 min followed by a solvothermal reaction at 200 °C for 2 h. After cooling down, the product was separated by centrifugation, washed with water and ethanol for three times, and dried at 70 °C for 24 h. The V₂O₅-HMs could be finally obtained after calcinating the blue precursor at 400 °C for 5 h in the air, with a heating rate of 3 °C min⁻¹. As a control experiment, V₂O₅-Ms were synthesized by the same procedure except for the addition of less amount of THAM. And when the solvent was changed into alcohol, the V₂O₅-NWs could be obtained.

Materials Characterization: XRD measurements were performed to investigate the crystallographic information using a D8 Discover X-ray diffractometer with a nonmonochromated Cu K α X-ray source. Field emission scanning electron microscopy images were collected with a JEOL-7100F SEM/EDS microscopy. TEM and HRTEM images were recorded by using a JEM-2100F microscope. BET surface areas were obtained by using Tristar II 3020 instrument.

Electrochemical Measurement: The electrochemical measurements were carried out using 2016 coin cells in a glove box filled with pure argon. The working electrodes were obtained using 60% V₂O₅-HM active material, 30% acetylene black, and 10% poly(tetrafluoroethylene). The mass loading of the electrode materials was 1.8–2.4 mg cm⁻². Lithium chips were used as the anode. The electrolyte was composed of 1 m LiPF₆ dissolved in EC/DMC with a volume ratio of 1:1. For full-cell assembly, the V₂O₅-HMs were used as cathode and the electrochemically lithiated Li₃VO₄-CNT composite was used as anode under the optimized mass loadings. It was also assembled using 2016 coin cells in a glove box with the electrolyte used in the half-cell. The capacity of the full-cell was calculated based on the mass of the V₂O₅ electrode. Galvanostatic charge/discharge measurements were performed using a multichannel battery testing system (LAND CT2001A). Cyclic voltammetry were recorded using an electrochemical workstation (CHI 760D).

Supporting Information

Supporting Information is available from the Wiley Online Library or from the author.

Acknowledgements

P.F.Z. and L.Z.Z. contributed equally to this work. This work was supported by the National Basic Research Program of China

(2013CB934103), the International Science & Technology Cooperation Program of China (2013DFA50840), the National Natural Science Foundation of China (51302203, 51272197), the National Natural Science Fund for Distinguished Young Scholars (51425204), the Hubei Province Natural Science Fund for Distinguished Young Scholars (2014CFA035), and the Fundamental Research Funds for the Central Universities (WUT: 2015-III-021, 2015-III-032, 2015-III-052, 2015-PY-2). Thanks to Prof. D. Y. Zhao of Fudan University, Prof. C. M. Lieber of Harvard University, and Prof. J. Liu of Pacific Northwest National Laboratory for strong support and stimulating discussions.

- [1] N. Recham, J. N. Chotard, L. Dupont, C. Delacourt, W. Walker, M. Armand, J. M. Tarascon, *Nat. Mater.* **2010**, *9*, 68.
- [2] D. L. Chao, X. H. Xia, J. L. Liu, Z. X. Fan, C. F. Ng, J. Y. Lin, H. Zhang, Z. X. Shen, H. J. Fan, *Adv. Mater.* **2014**, *26*, 5794.
- [3] K. Kang, Y. S. Meng, J. Breger, C. P. Grey, G. Ceder, *Science* **2006**, *311*, 977.
- [4] C. Wang, W. Wan, Y. H. Huang, J. T. Chen, H. H. Zhou, X. X. Zhang, *Energy Environ. Sci.* **2014**, *7*, 1680.
- [5] J. M. Tarascon, M. Armand, *Nature* **2001**, *414*, 359.
- [6] S. Q. Wang, S. R. Li, Y. Sun, X. Y. Feng, C. H. Chen, *Energy Environ. Sci.* **2011**, *4*, 2854.
- [7] P. G. Bruce, S. A. Freunberger, L. J. Hardwick, J. M. Tarascon, *Nat. Mater.* **2012**, *11*, 19.
- [8] B. Kang, G. Ceder, *Nature* **2009**, *458*, 190.
- [9] M. Armand, J. M. Tarascon, *Nature* **2008**, *451*, 652.
- [10] N. Mahmood, C. Z. Zhang, F. Liu, J. H. Zhu, Y. L. Hou, *ACS Nano* **2013**, *7*, 10307.
- [11] K. T. Lee, R. Black, T. Yim, X. L. Ji, L. F. Nazar, *Adv. Energy Mater.* **2012**, *2*, 1490.
- [12] S. Q. Wang, S. R. Li, Y. Sun, X. Y. Feng, C. H. Chen, *Energy Environ. Sci.* **2011**, *4*, 2854.
- [13] H. Wu, G. Chan, J. W. Choi, I. Ryu, Y. Yao, M. T. McDowell, S. W. Lee, A. Jackson, Y. Yang, L. B. Hu, Y. Cui, *Nat. Nanotechnol.* **2012**, *7*, 309.
- [14] C. Z. Yuan, H. B. Wu, Y. Xie, X. W. Lou, *Angew. Chem. Int. Ed.* **2013**, *52*, 2.
- [15] N. Liu, H. Wu, M. T. McDowell, Y. Yao, C. M. Wang, Y. Cui, *Nano Lett.* **2012**, *12*, 3315.
- [16] J. Liu, H. Xia, D. F. Xue, L. Lu, *J. Am. Chem. Soc.* **2009**, *131*, 12086.
- [17] L. Q. Mai, Q. Y. An, Q. L. Wei, J. Y. Fei, P. F. Zhang, X. Xu, Y. L. Zhao, M. Y. Yan, W. Wen, L. Xu, *Small* **2014**, *10*, 3032.
- [18] J. Shao, X. Y. Li, Z. M. Wan, L. F. Zhang, Y. L. Ding, L. Zhang, Q. T. Qu, H. H. Zheng, *ACS Appl. Mater. Interfaces* **2013**, *5*, 7671.
- [19] Y. Y. Liu, M. Clark, Q. F. Zhang, D. M. Yu, D. W. Liu, J. Liu, G. Z. Cao, *Adv. Energy Mater.* **2011**, *1*, 194.
- [20] M. S. Whittingham, *Chem. Rev.* **2004**, *104*, 4271.
- [21] Y. Wang, K. Takahashi, K. Lee, G. Z. Cao, *Adv. Funct. Mater.* **2006**, *16*, 1133.
- [22] X. F. Zhang, K. X. Wang, X. Wei, J. S. Chen, *Chem. Mater.* **2011**, *23*, 5290.
- [23] X. Y. Chen, H. L. Zhu, Y. C. Chen, Y. Y. Shang, A. Y. Cao, L. B. Hu, G. W. Rubloff, *ACS Nano* **2012**, *6*, 7948.
- [24] W. J. Wang, H. Y. Wang, S. Q. Liu, J. H. Huang, *J. Solid State Electrochem.* **2012**, *16*, 2555.
- [25] Y. Wang, G. Z. Cao, *Adv. Mater.* **2008**, *20*, 2251.
- [26] H. Wang, K. Huang, C. Huang, S. Liu, Y. Ren, X. Huang, *J. Power Sources* **2011**, *196*, 5645.
- [27] T. Y. Zhai, H. M. Liu, H. Q. Li, X. S. Fang, M. Y. Liao, L. Li, H. S. Zhou, Y. S. Koide, Y. S. Bando, D. Golberg, *Adv. Mater.* **2010**, *22*, 2547.
- [28] Y. H. Wang, Y. H. Wang, D. S. Jia, Z. Peng, Y. Y. Xia, G. F. Zheng, *Nano Lett.* **2014**, *14*, 1080.
- [29] S. Q. Wang, Z. D. Lu, D. Wang, C. G. Li, C. H. Chen, Y. D. Yin, *J. Mater. Chem.* **2011**, *21*, 6365.
- [30] H. K. Koduru, H. M. Obili, G. Cecilia, *Int. Nano Lett.* **2013**, *3*, 24.
- [31] X. F. Zhang, K. X. Wang, X. Wei, J. S. Chen, *Chem. Mater.* **2011**, *23*, 5290.
- [32] H. Q. Song, C. P. Zhang, Y. G. Liu, C. F. Liu, X. H. Nan, G. Z. Cao, *J. Power Sources* **2015**, *294*, 1.
- [33] Y. K. Sun, S. M. Oh, H. K. Park, B. Scrosati, *Adv. Mater.* **2011**, *23*, 5050.
- [34] N. Liu, Z. D. Lu, J. Zhao, M. T. McDowell, H. Lee, W. T. Zhao, Y. Cui, *Nat. Nanotech.* **2014**, *9*, 187.
- [35] C. F. Zhang, Z. X. Chen, Z. P. Guo, X. W. Lou, *Energy Environ. Sci.* **2013**, *6*, 974.
- [36] A. M. Cao, J. S. Hu, H. P. Liang, L. J. Wan, *Angew. Chem. Int. Ed.* **2005**, *44*, 4391.
- [37] H. B. Wu, A. Q. Pan, H. H. Hng, X. W. Lou, *Adv. Funct. Mater.* **2013**, *23*, 5669.
- [38] A. Q. Pan, H. B. Wu, L. Yu, X. W. Lou, *Angew. Chem.* **2013**, *125*, 2282.
- [39] E. Uchaker, N. Zhou, Y. W. Li, G. Z. Cao, *J. Phys. Chem. C* **2013**, *117*, 1621.
- [40] Y. H. Wang, Y. H. Wang, D. S. Jia, Z. Peng, Y. Y. Xia, G. F. Zheng, *Nano Lett.* **2014**, *14*, 1080.
- [41] L. S. Plashnitsa, E. Kobayashi, Y. Noguchi, S. Okada, J. Yamaki, *J. Electrochem. Soc.* **2010**, *157*, A536.
- [42] D. Su, G. Wang, *ACS Nano* **2013**, *7*, 11218.
- [43] Q. D. Li, J. Z. Sheng, Q. L. Wei, Q. Y. An, X. J. Wei, P. F. Zhang, L. Q. Mai, *Nanoscale* **2014**, *6*, 11072.
- [44] B. Vigolo, C. Zakri, F. Nallet, J. Livage, C. Coulon, *Langmuir* **2002**, *18*, 9121.
- [45] J. Livage, *Chem. Mater.* **1991**, *3*, 578.
- [46] R. Tenne, *Nat. Nanotechnol.* **2006**, *1*, 103.
- [47] N. E. Good, G. D. Winget, W. Winter, T. N. Connolly, S. Izawa, R. M. M. Singh, *Biochemistry* **1966**, *5*, 467.
- [48] M. Taha, M. J. Lee, *Biochem. Eng. J.* **2009**, *46*, 334.
- [49] Q. Y. An, Q. L. Wei, P. F. Zhang, J. Z. Sheng, K. M. Hercule, F. Lv, Q. Q. Wang, X. J. Wei, L. Q. Mai, *Small* **2015**, *11*, 2654.
- [50] M. Jaber, F. O. Ribot, L. Binet, V. R. Briois, S. Cassaignon, K. Rao, J. Livage, N. Steunou, *J. Phys. Chem. C* **2012**, *116*, 25126.
- [51] D. McNulty, D. N. Buckley, C. O'Dwyer, *J. Power Sources* **2014**, *267*, 831.
- [52] Q. L. Wei, S. S. Tan, X. Y. Liu, M. Y. Yan, F. C. Wang, Q. D. Li, Q. Y. An, R. M. Sun, K. N. Zhao, H. A. Wu, L. Q. Mai, *Adv. Funct. Mater.* **2015**, *25*, 1773.
- [53] Q. Y. An, Q. L. Wei, L. Q. Mai, J. Y. Fei, X. Xu, Y. L. Zhao, M. Y. Yan, P. F. Zhang, S. Z. Huang, *Phys. Chem. Chem. Phys.* **2013**, *15*, 16828.
- [54] Q. Y. An, P. F. Zhang, Q. L. Wei, L. He, F. Y. Xiong, J. Z. Sheng, Q. Q. Wang, L. Q. Mai, *J. Mater. Chem. A* **2014**, *2*, 3297.
- [55] Y. Yao, M. T. McDowell, I. Ryu, H. Wu, N. Liu, L. B. Hu, W. D. Nix, Y. Cui, *Nano Lett.* **2011**, *11*, 2949.
- [56] J. Jiang, Y. Li, J. Liu, X. Huang, C. Yuan, X. W. Lou, *Adv. Mater.* **2012**, *24*, 5166.
- [57] N. Jayaprakash, J. Shen, S. S. Moganty, A. Corona, L. A. Archer, *Angew. Chem. Int. Ed.* **2011**, *50*, 5904.
- [58] X. F. Li, H. M. Zhang, Z. S. Mai, H. Z. Zhang, I. Vankelecom, *Energy Environ. Sci.* **2011**, *4*, 1147.
- [59] L. B. Hu, N. Liu, M. Eskilsson, G. Y. Zheng, J. McDonough, L. Wagberg, Y. Cui, *Nano Energy* **2013**, *2*, 138.
- [60] L. B. Hu, H. Wu, Y. F. Gao, A. Y. Cao, H. B. Li, J. McDough, X. Xie, M. Zhou, Y. Cui, *Adv. Energy Mater.* **2011**, *1*, 523.

- [61] R. Y. Zhang, Y. J. Du, D. Li, D. K. Shen, J. P. Yang, Z. P. Guo, H. K. Liu, A. A. Elzatahry, D. Y. Zhao, *Adv. Mater.* **2014**, *26*, 6749.
- [62] D. Y. Chen, X. Mei, G. Ji, M. H. Lu, J. P. Xie, J. M. Lu, J. Y. Lee, *Angew. Chem. Int. Ed.* **2012**, *51*, 2409.
- [63] H. Q. Li, X. Z. Liu, T. Y. Zhai, D. Li, H. S. Zhou, *Adv. Energy Mater.* **2013**, *3*, 428.
- [64] Y. Shi, J. Z. Wang, S. L. Chou, D. Wexler, H. J. Li, K. Ozawa, H. K. Liu, Y. P. Wu, *Nano Lett.* **2013**, *13*, 4715.
- [65] C. K. Zhang, H. Q. Song, C. F. Liu, Y. G. Liu, C. P. Zhang, X. H. Nan, G. Z. Cao, *Adv. Funct. Mater.* **2015**, *25*, 3497.
- [66] T. Nordh, R. Younesi, D. Brandell, K. Edström, *J. Power Sources* **2015**, *294*, 173.
- [67] S. Bae, I. Nam, S. Park, Y. G. Yoo, S. Yu, J. M. Lee, J. W. Han, J. Yi, *ACS Appl. Mater. Interfaces* **2015**, *7*, 16565.
- [68] V. Petkov, P. N. Trikalitis, E. S. Bozin, S. J. Billinge, T. Vogt, M. G. Kanatzidis, *J. Am. Chem. Soc.* **2002**, *124*, 10157.

Received: October 24, 2015
Revised: November 29, 2015
Published online: January 4, 2016